

Supporting Information

Triazole appending ruthenium (II) polypyridine complex for selective sensing of phosphate anions through C-H---anion interaction and copper (II) ions via cancer cells

Mohanraj Ramachandran ^a and Sambandam Anandan ^{*a}

^aDepartment of Chemistry, National Institute of Technology, Tiruchirappalli 620 015, India

TABLE OF CONTENT

No.	Content	Fig. No.	Page. No.
1.	^1H NMR spectrum of 1 in CDCl_3	Fig. S1	5
2.	^{13}C NMR spectrum of 1 in CDCl_3	Fig. S2	5
3.	^1H NMR spectrum of 2 in CDCl_3	Fig. S3	6
4.	^{13}C NMR spectrum of 2 in CDCl_3	Fig. S4	6
5.	^1H NMR spectrum of Btb in CDCl_3	Fig. S5	7
6.	^{13}C NMR spectrum of Btb in CDCl_3	Fig. S6	7
7.	^1H NMR spectrum of Rbtb in DMSO-d_6	Fig. S7	8
8.	Expanded ^1H NMR spectrum of Rbtb in DMSO-d_6	Fig. S8	8
9.	^1H NMR spectrum of Rbtb in CD_3CN	Fig. S9	9
10.	^{13}C NMR spectrum of Rbtb in CD_3CN	Fig. S10	9
11.	MALDI-TOF Mass spectrum of Btb	Fig. S11	10
12.	MALDI-TOF Mass spectrum of Rbtb	Fig. S12	10
13.	FT-IR spectra for compound 1, 2 (ATR Mode), Btb and Rbtb	Fig. S13	11
14.	(A) UV-Vis spectra of Rbtb with gradual addition of two equiv. of H_2PO_4^- (B) UV-Vis spectra of Rbtb with gradual addition of two equiv. of $\text{H}_2\text{P}_2\text{O}_7^{2-}$	Fig. S14	11
15.	(A) Interference study of Rbtb- H_2PO_4^- with mentioned anions (B) Interference study of Rbtb- $\text{H}_2\text{P}_2\text{O}_7^{2-}$ with mentioned anions	Fig. S15	11
16.	(A) Job's plot for Rbtb- H_2PO_4^- (B) Job's plot for Rbtb- $\text{H}_2\text{P}_2\text{O}_7^{2-}$	Fig. S16	12
17.	(A) Under UV light illumination, Rbtb with mentioned anions (B) Under UV light illumination, Rbtb with mentioned metal ions	Fig. S17	12
18.	NMR titration of Rbtb with H_2PO_4^- in $\text{CD}_3\text{CN}/\text{CD}_3\text{OD}$	Fig. S18	13
19.	(A) UV-Vis spectra of Rbtb with variety of metal ions (B) UV-Vis spectra of Rbtb with gradual addition of two equiv. of Cu^{2+} ions	Fig. S19	13
20.	(A) Interference study of Rbtb- Cu^{2+} with mentioned metal ions (B) linear plot of Rbtb- Cu^{2+}	Fig. S20	13
21.	Stern-Volmer plot for the detection of Cu^{2+} ion by relative fluorescence Rbtb in $\text{CH}_3\text{CN}/10\text{mM}$ HEPES buffer ($\text{pH} = 7.4$).	Fig. S21	14
22.	pH variation was monitored with Rbtb, Rbtb- Cu^{2+}	Fig. S22	14
23.	The cyclic voltammogram of Rbtb, with phosphate and with copper (II) ions	Fig. S23	14
24.	Optimized geometry of Rbtb	Fig. S24	15

25.	Mass spectrum of [Rbtb-Cu ²⁺] adduct	Fig. S25	15
26.	Job's plot for Rbtb-Cu ²⁺	Fig. S26	15
27.	EPR Spectra of Rbtb+Cu ²⁺ at LNT	Fig. S27	16
28.	Proposed mechanism of Rbtb-H ₂ PO ₄ ⁻ and Rbtb-Cu ²⁺	Fig. S28	16
29.	DAPI staining	Fig. S29	17
30.	Comparative table for detection limit	Table. S1	17
31.	References	-	18

Synthetic procedure of compound 1 and 2

2-(2-propynyloxy)-1,3-benzothiazole (1)^{S1}

In 100 ml round bottom flask, 2-hydroxybenzothiazole (1.208 g, 8 mmol), propargyl bromide (1.764 g, 12 mmol) and potassium carbonate (1.656 g, 12 mmol) in acetone (50 mL) was stirred for 4 h. After constant stirring, the solvent was evaporated using a rotatory evaporator. Then distilled water (30 mL) and dichloromethane (30 mL) was added to the reaction mixture and transferred to a separating funnel. The product was extracted into the organic layer, isolated and dried over sodium sulphate. Impure product was obtained upon the organic solvent was removed under reduced pressure and it was purified using flash column chromatography to get off white solid as 1 (1.347 g, 89 %). ¹H NMR (CDCl₃, 500 MHz, ppm): δ = 7.44 (dd, 7.53 Hz, 1H), 7.36 (dd, 7.54 Hz, 1H), 7.25 (td, 8.54 Hz, 1H), 7.20 (td, 8.54 Hz, 1H), 4.76 (s, 2H), 2.30 (s, 1H). ¹³C NMR (CDCl₃, 150 MHz, ppm); δ = 169.38, 136.06, 125.50, 123.64, 122.68, 122.41, 111.17, 73.19 and 31.68.

4-azido-2,2'-bipyridyl (2)^{S2,S3}

4-nitro-2,2'-bipyridyl (0.57 g, 0.4 mmol, 1 eq.) with NaN₃ (1.50 g, 3.85 mmol, 8.95 eq.) was heated in DMF (10 mL) for 5 hours at 100 °C. The solvent was removed under vacuum and water (40 mL) was added to the yellow solid, the aqueous phase was extracted with dichloromethane. The combined organic phase was dried over anhydrous sodium sulphate. The crude product was purified by flash silica column chromatography using dichloromethane/ethyl acetate (1:1) mixture. The yellow colour solid was obtained as 4-azido-2,2'-bipyridyl (yield, 0.52g, 93.54 %). ¹H NMR (CDCl₃) δ (ppm): 8.69 (ddd, J = 4.8, 1.8 & 0.9 Hz, 1H, H-6'), 8.58 (d, J = 5.4 Hz, 1H, H-6), 8.40 (dt, J = 7.8 & 0.9 Hz, 1H, H-4'), 8.15 (d, J = 2.3 Hz, 1H, H-3), 7.82 (td, J = 7.8 & 1.8, 1H, H-5'), 7.34 (ddd, J = 7.5, 4.8 & 1.2, 1H, H-3'), 6.93 (dd, J = 5.4 & 2.3 Hz, 1H, H-5). (¹³C NMR, 100 MHz) δ (ppm): 162.5, 149.4, 148.8, 141.8, 138.4, 136.4, 125.6, 124.7, 117.5, 116.1. FT-IR (ATR): 2115 cm⁻¹ (s).

Determination of the detection limit

The detection limit (LOD) of Rbtb towards anions and cation was calculated by $3\sigma/S$, where σ is the standard deviation of the blank studies and S is the slope of the calibration curve.

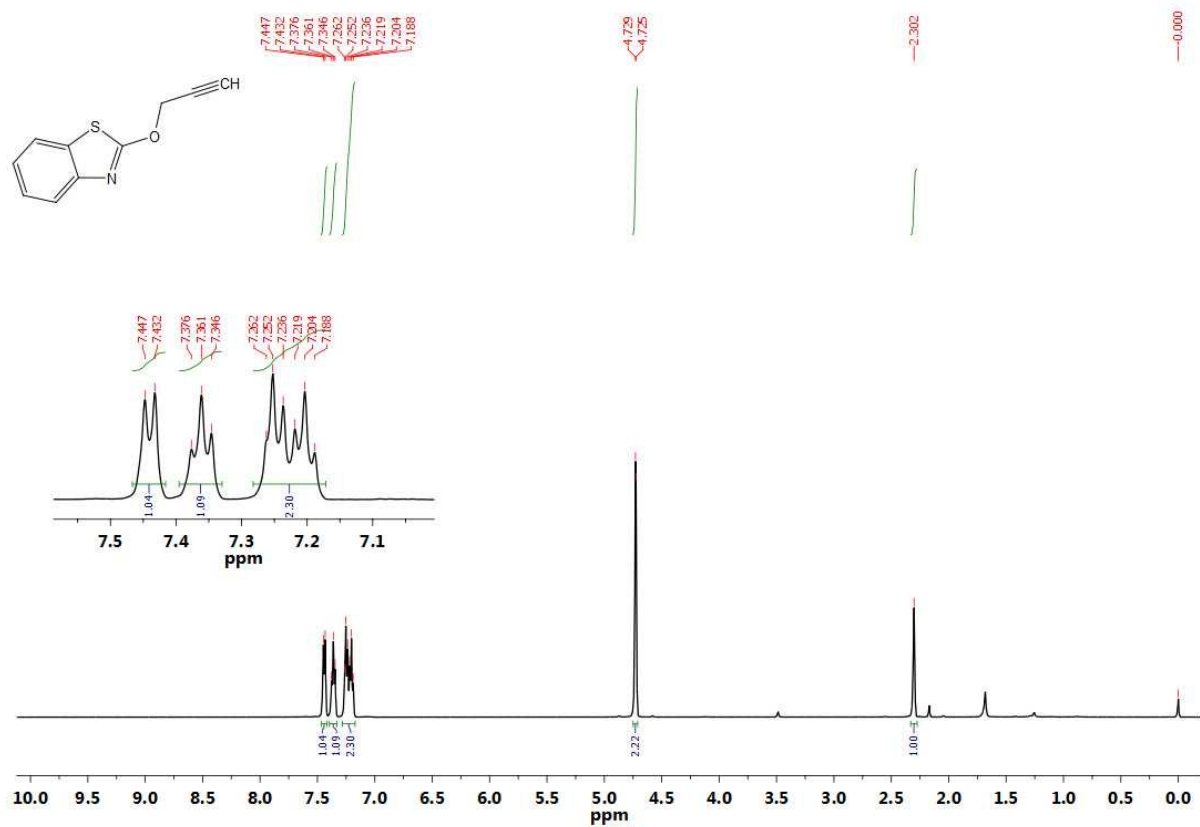


Fig. S1 ¹H NMR spectrum of **1** in CDCl₃

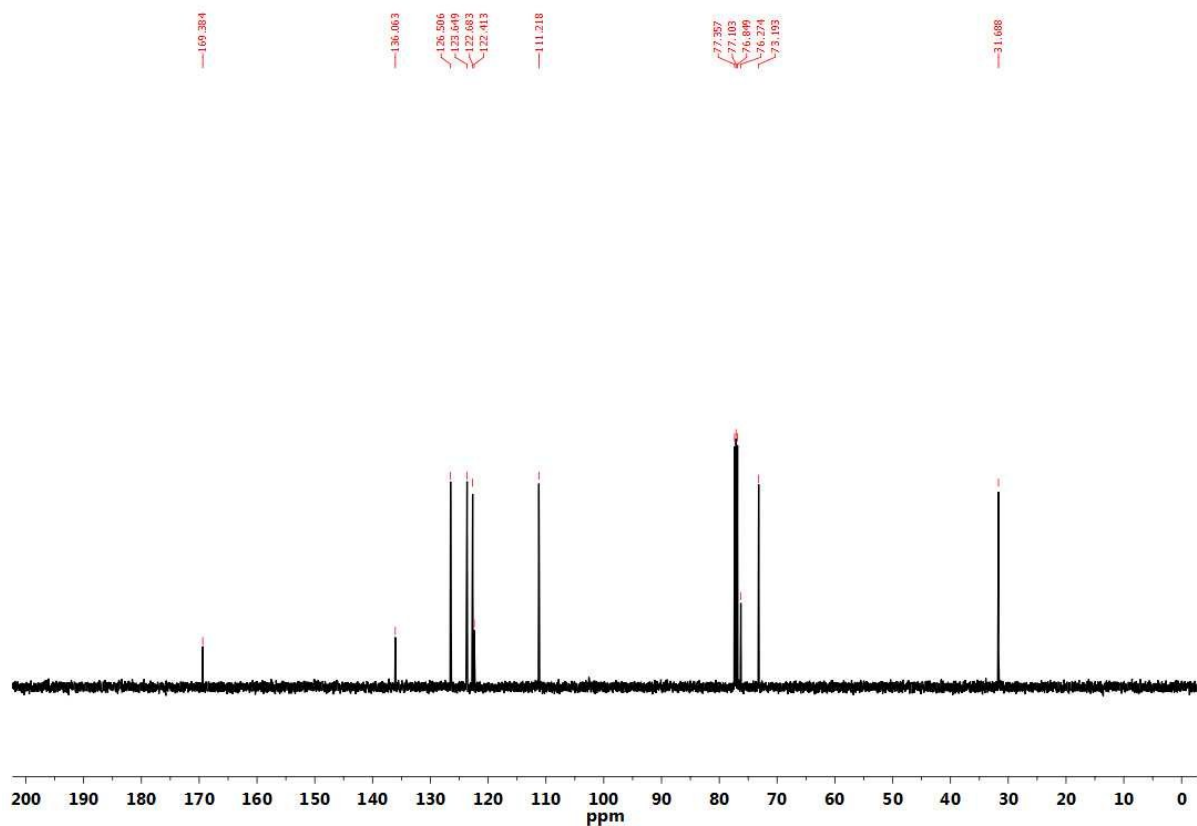
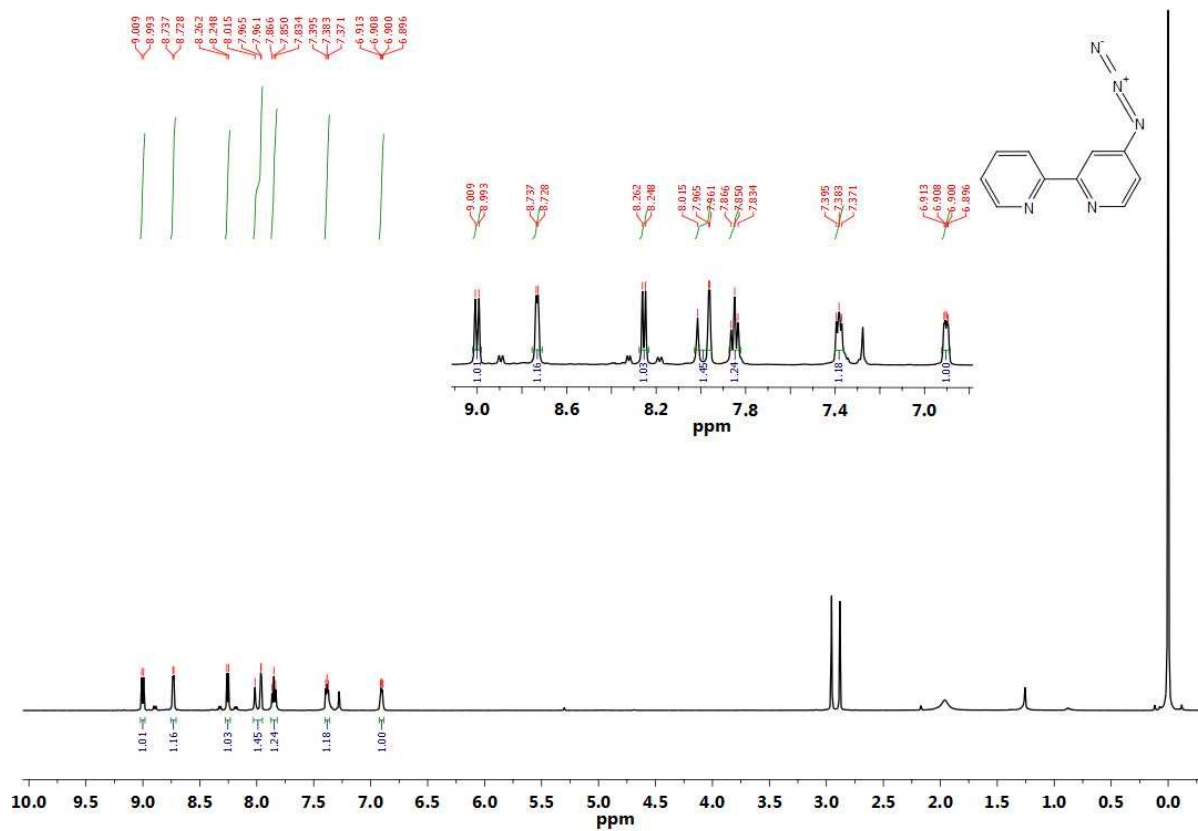


Fig. S2 ¹³C NMR spectrum of **1** in CDCl₃



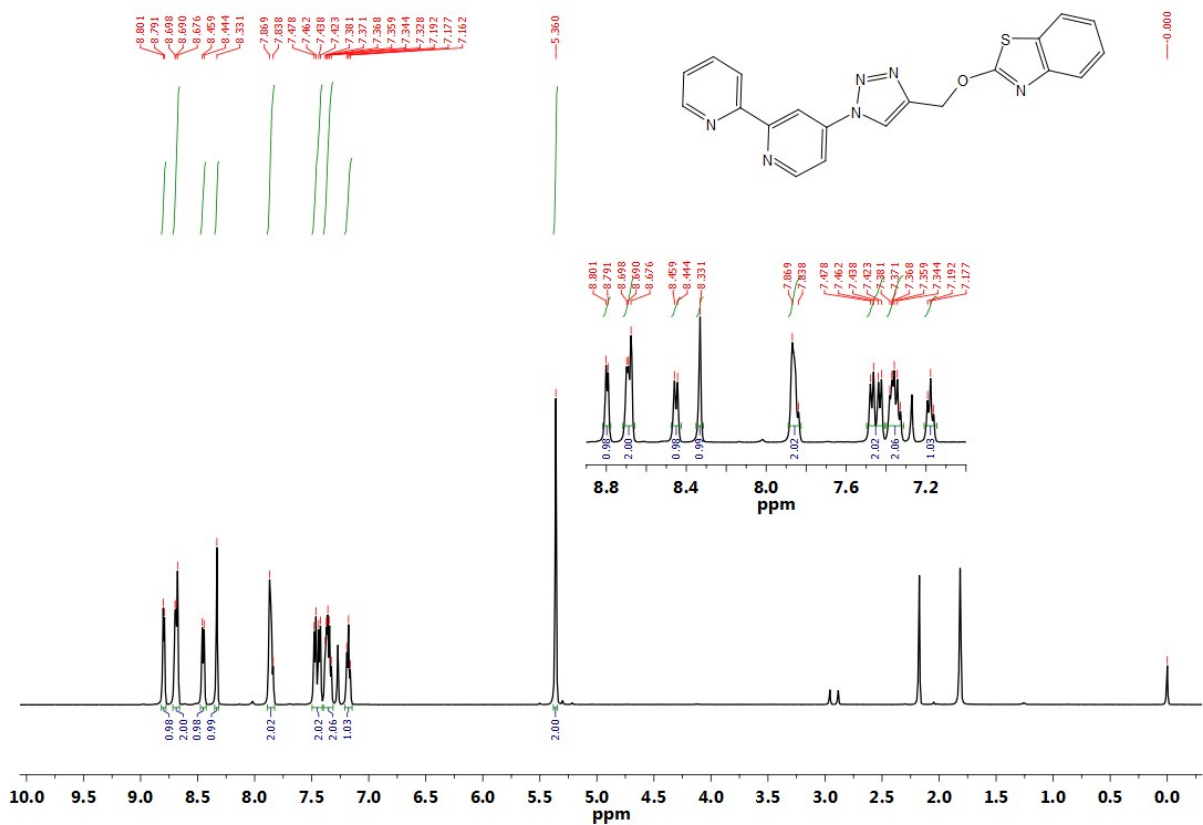


Fig. S5 ¹H NMR spectrum of Btb in CDCl₃

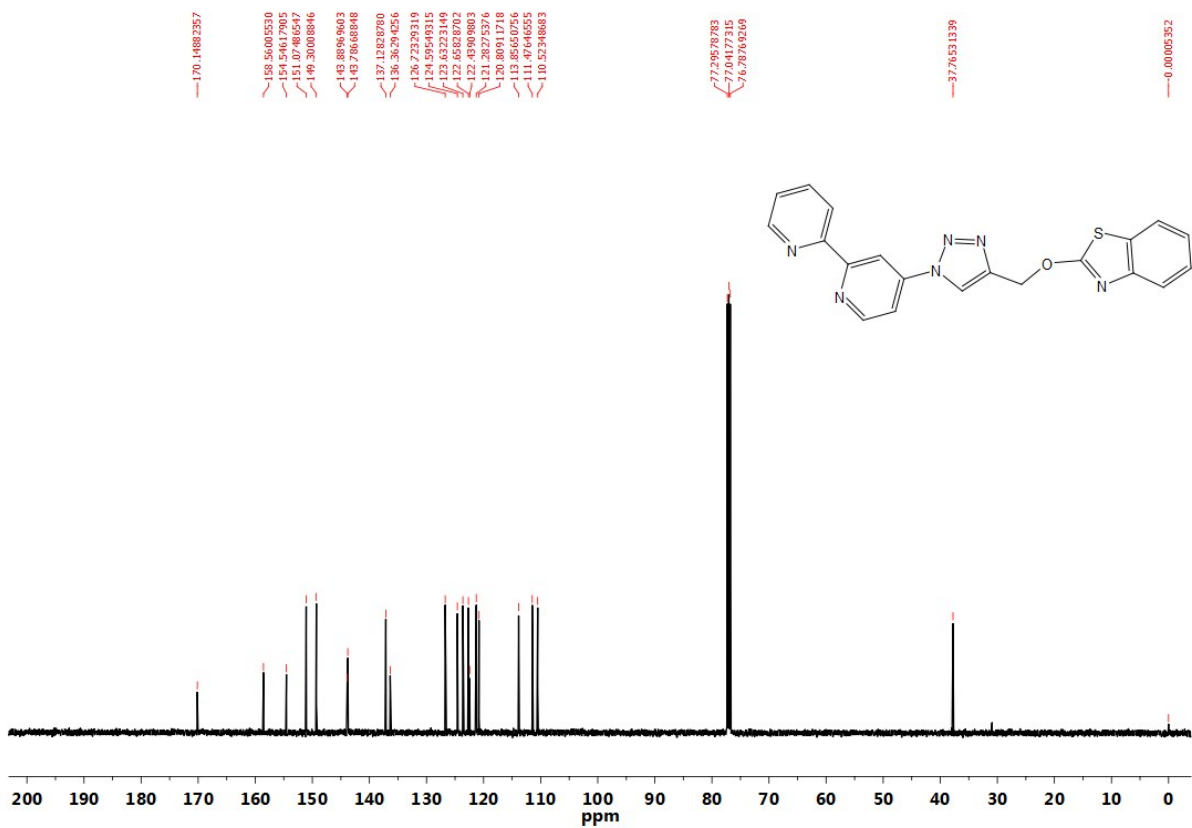


Fig. S6 ¹³C NMR spectrum of Btb in CDCl₃

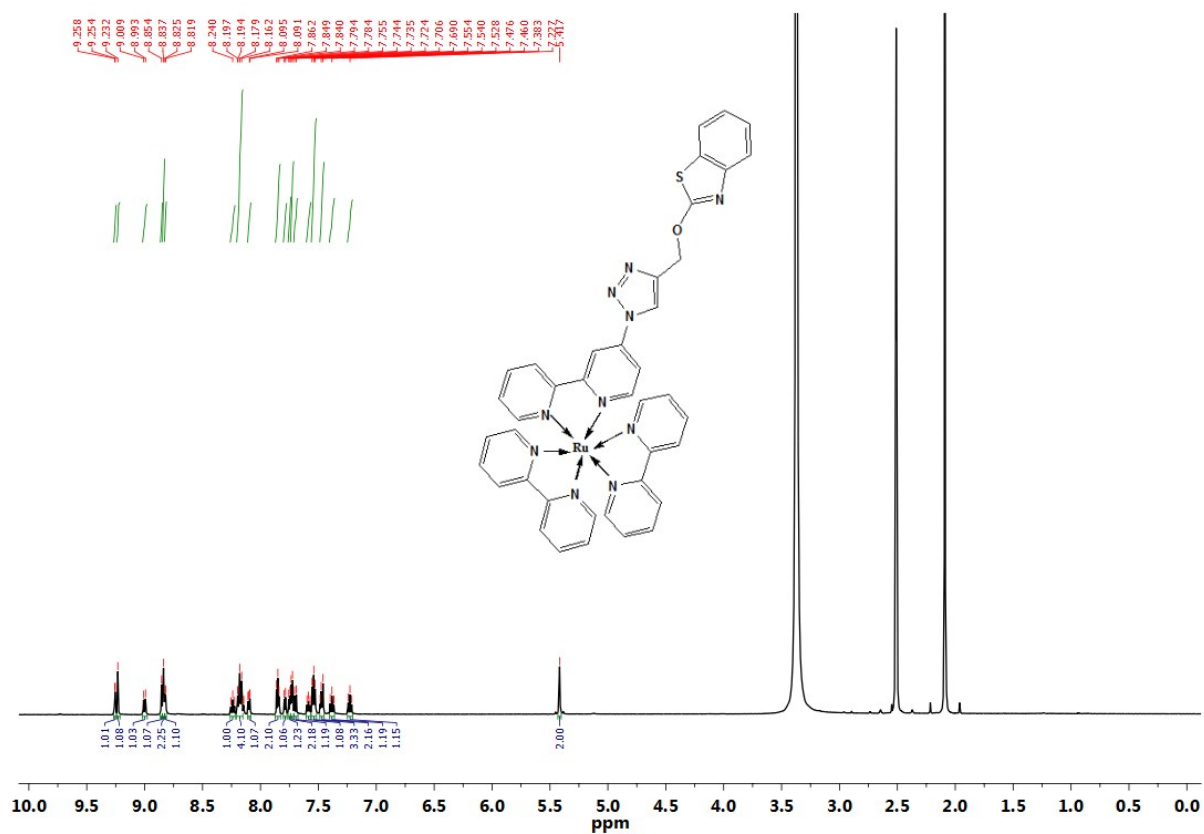


Fig. S7 ^1H NMR spectrum of **Rbtb** in DMSO-d_6

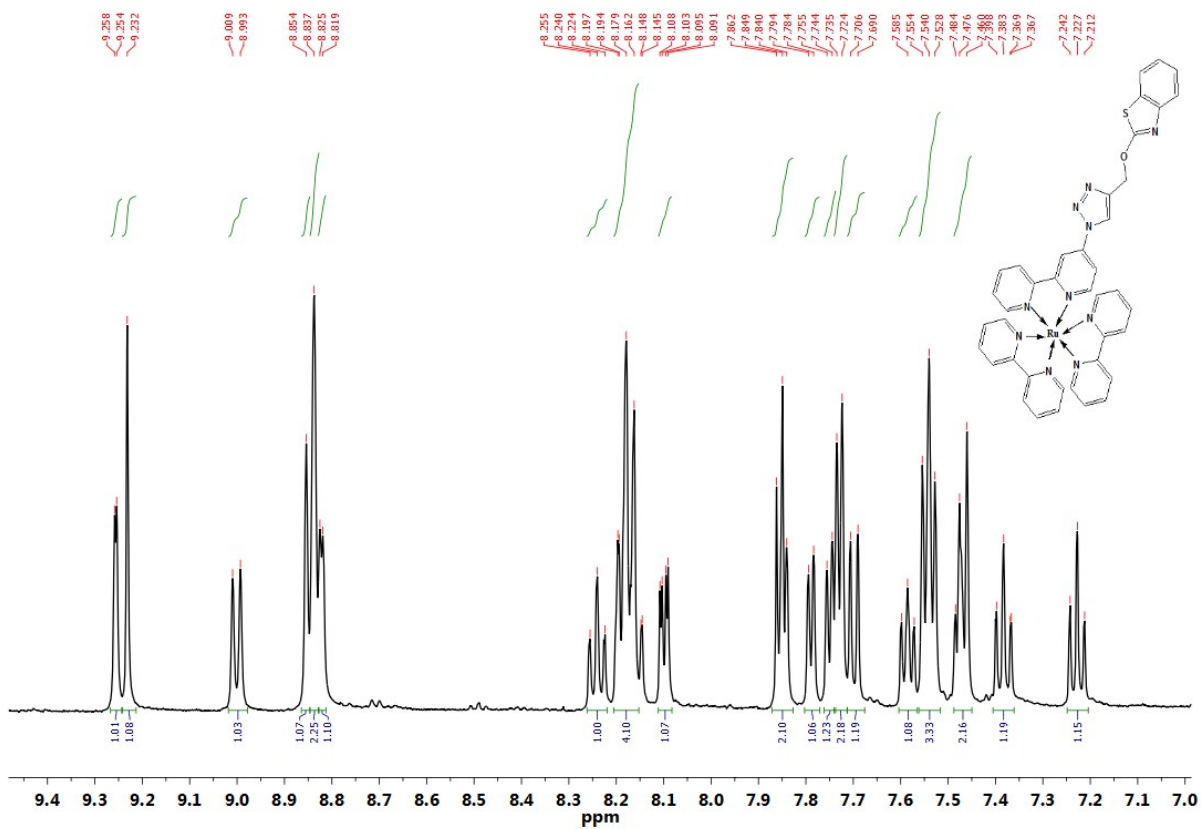


Fig. S8 Expanded ^1H NMR spectrum of **Rbtb** in DMSO-d_6

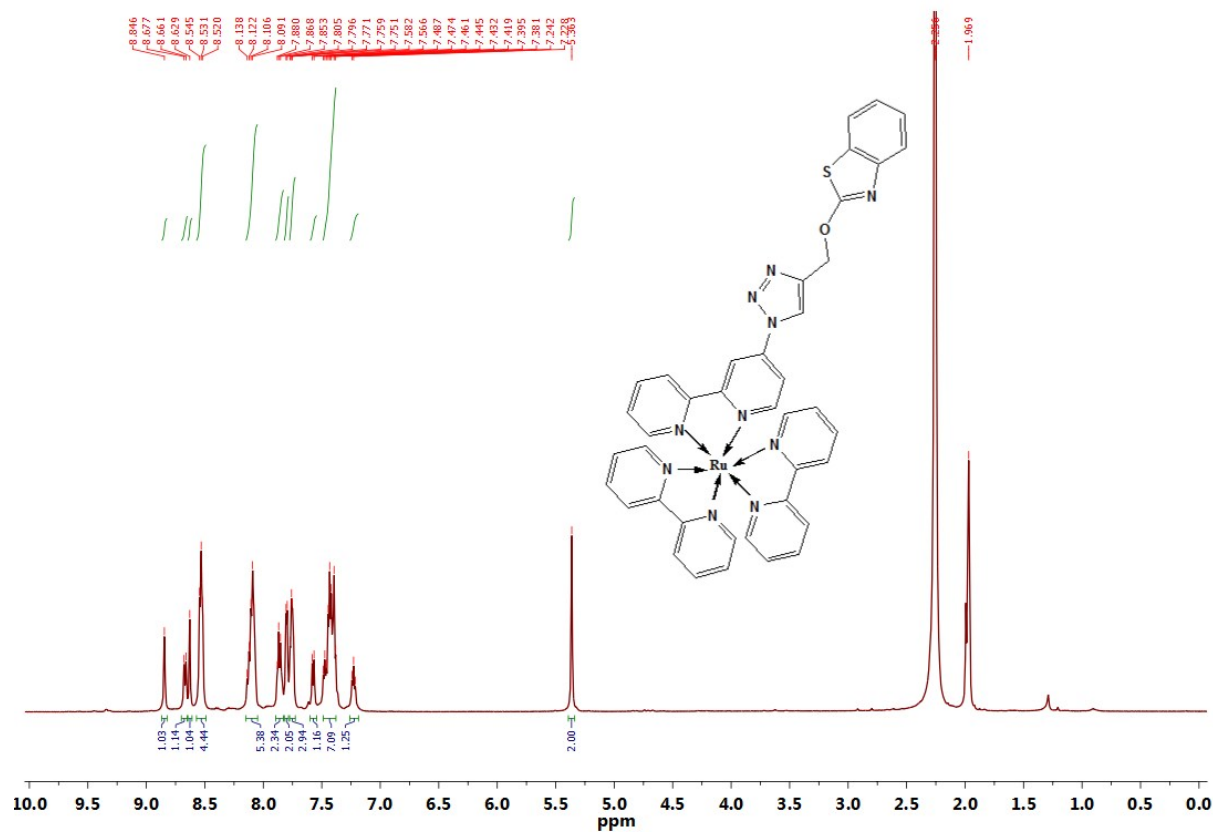


Fig. S9 ^1H NMR spectrum of Rbtb in CD_3CN

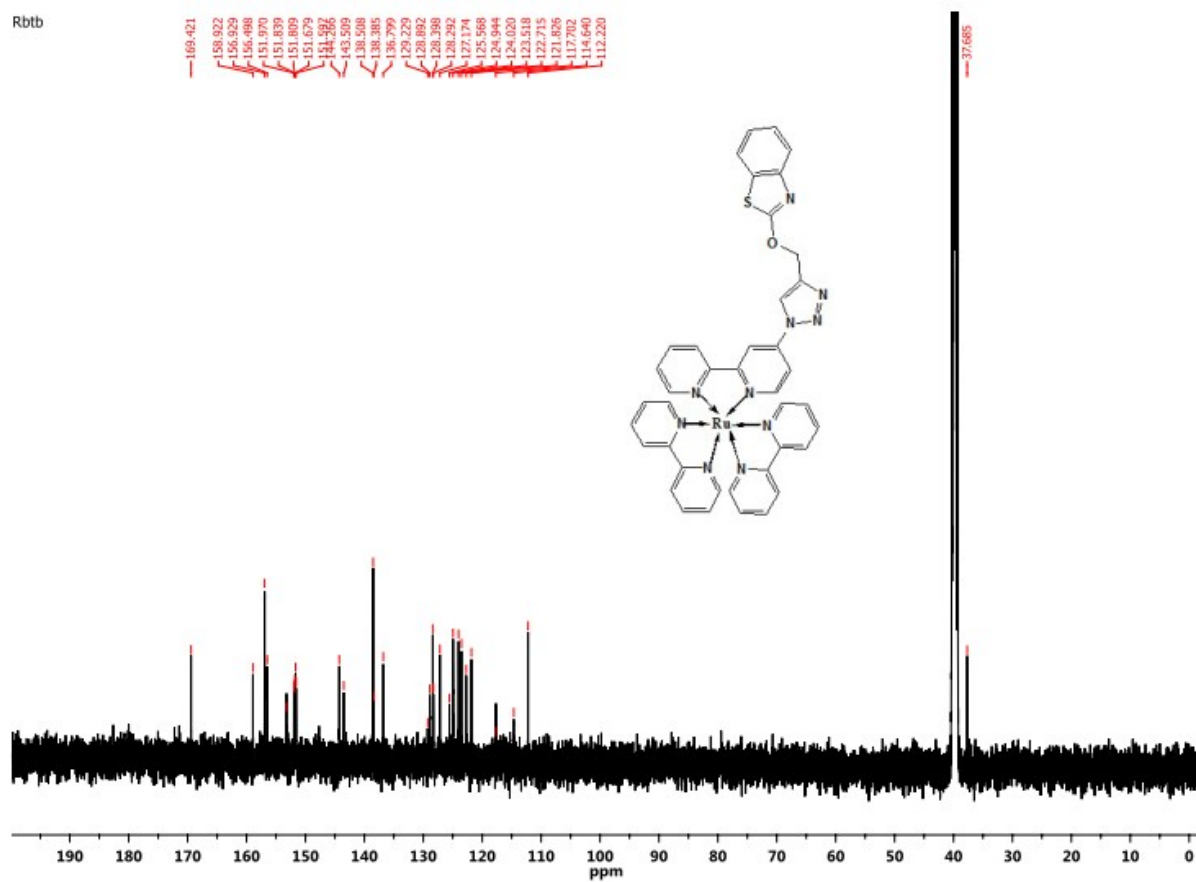


Fig. S10 ^{13}C NMR spectrum of Rbtb in DMSO-d_6

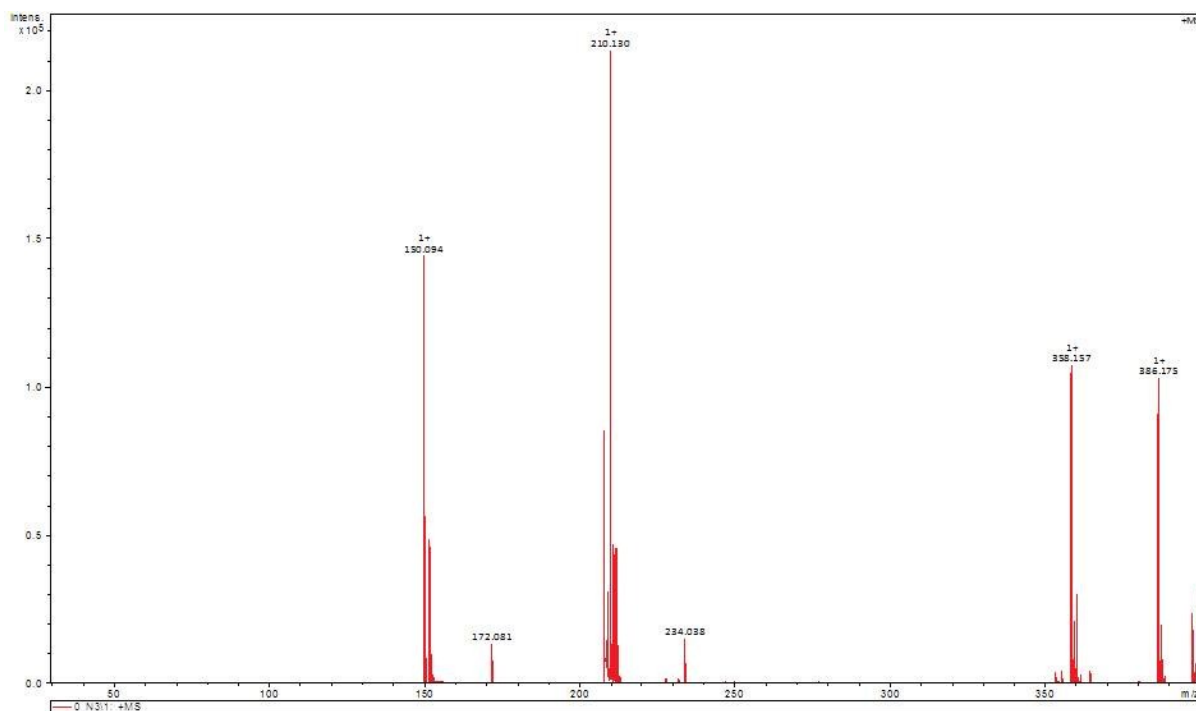


Fig. S11 MALDI-TOF Mass spectrum of **Btb**

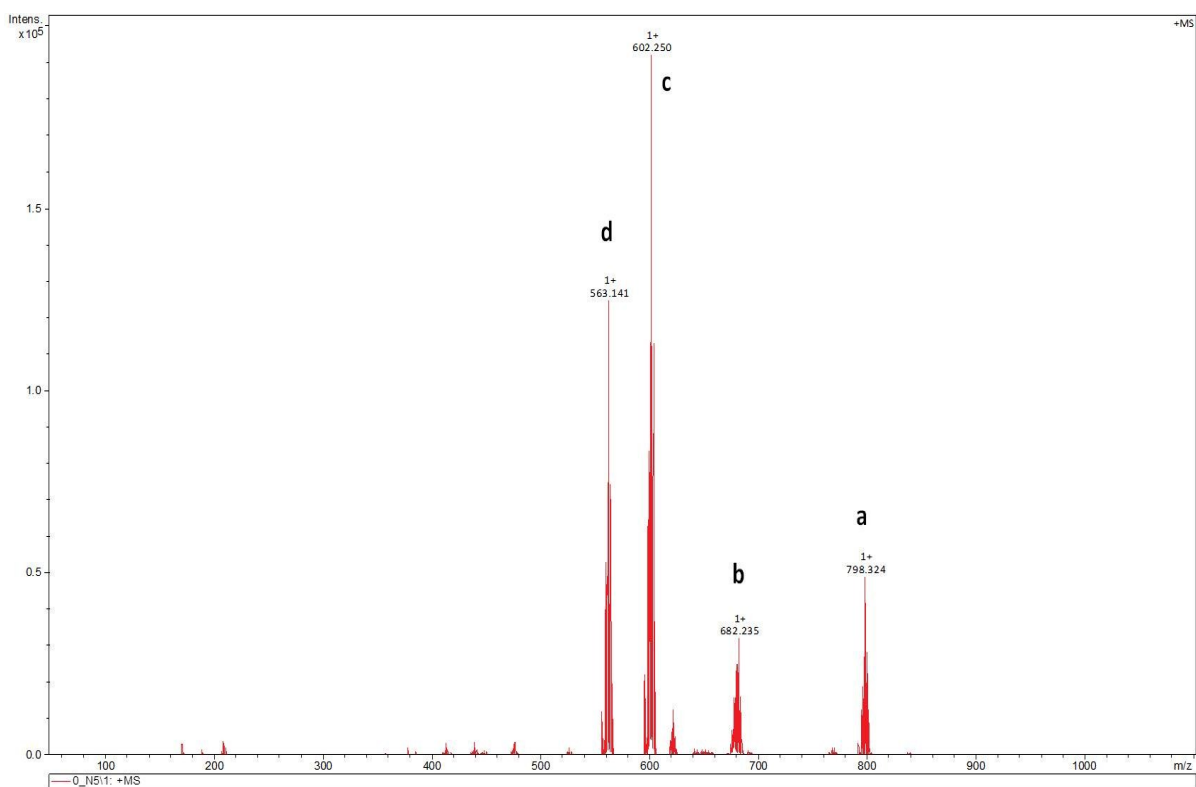


Fig. S12 MALDI-TOF Mass spectrum of **Rbtb** {a = $[M-H]^+$ ($M = C_{40}H_{30}N_{10}OSRu$), b = $[M+H]^+$ ($M = C_{34}H_{29}N_9ORu$), c = $[M+2H]^+$ ($M = C_{30}H_{26}N_8Ru$), d = $[M+K]^+$ ($M = C_{24}H_{21}N_7ORu$)}

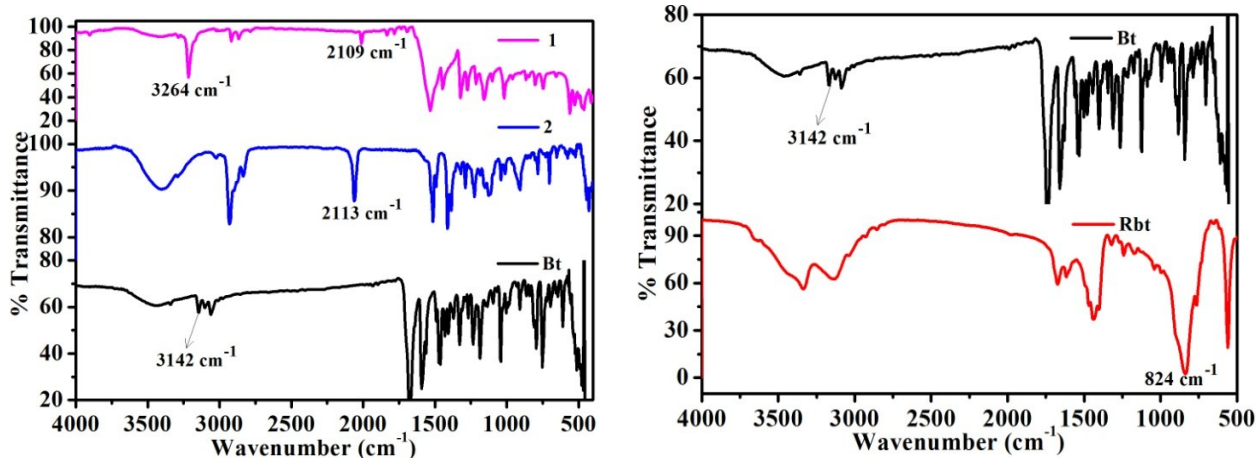


Fig. S13 FT-IR spectra of 1, 2, Btb and Rbtb

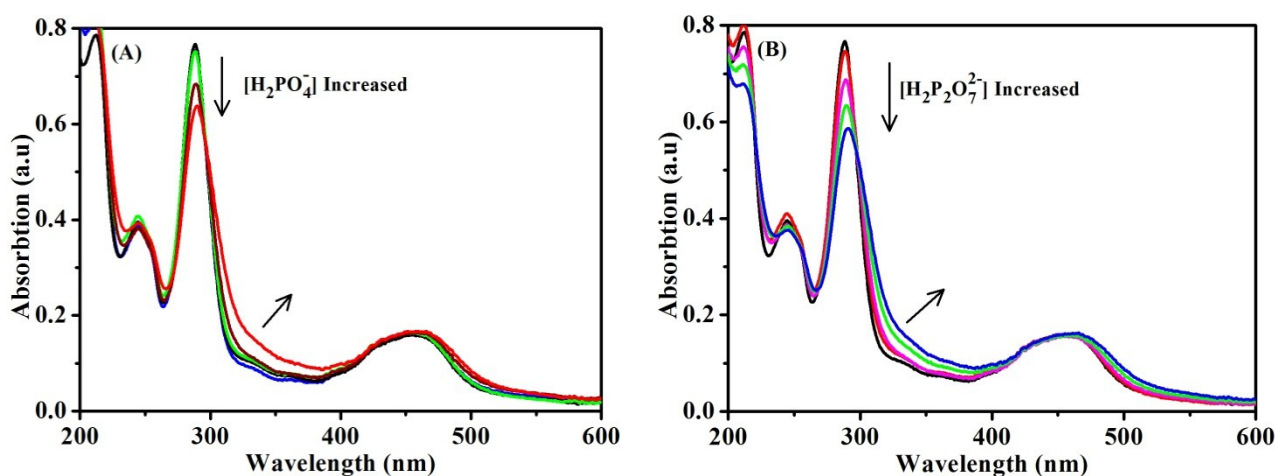


Fig. S14 (A) UV-Vis spectra of Rbtb (10 μM) with the gradual addition of two equiv. of H_2PO_4^- (B) UV-Vis spectra of Rbtb (10 μM) with the gradual addition of two equiv. of $\text{H}_2\text{P}_2\text{O}_7^{2-}$

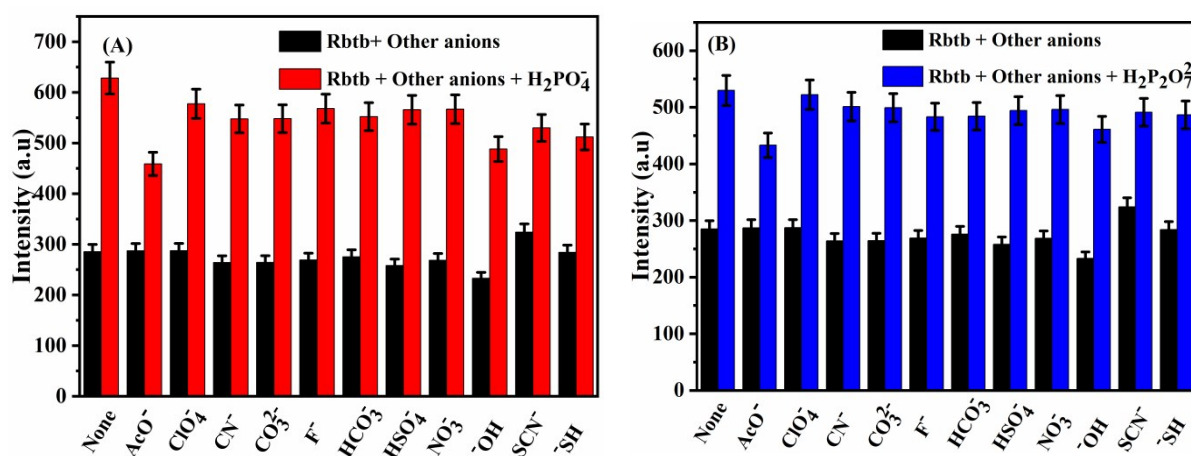


Fig. S15 (A) Interference study of Rbtb (10 μM) + H_2PO_4^- (2 equiv.) with mentioned other anions (10 equiv.) (B) Interference study of Rbtb (10 μM) + $\text{H}_2\text{P}_2\text{O}_7^{2-}$ (2 equiv.) with mentioned other anions (10 equiv.).

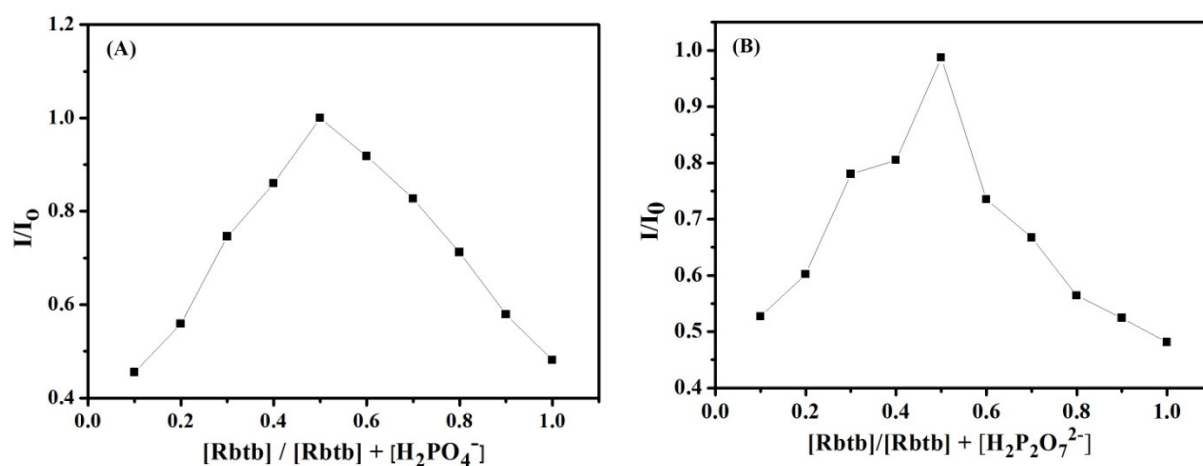


Fig. S16. (A) Job's plot for Rbtb- $H_2PO_4^-$ (B) Job's plot for Rbtb- $H_2P_2O_7^{2-}$

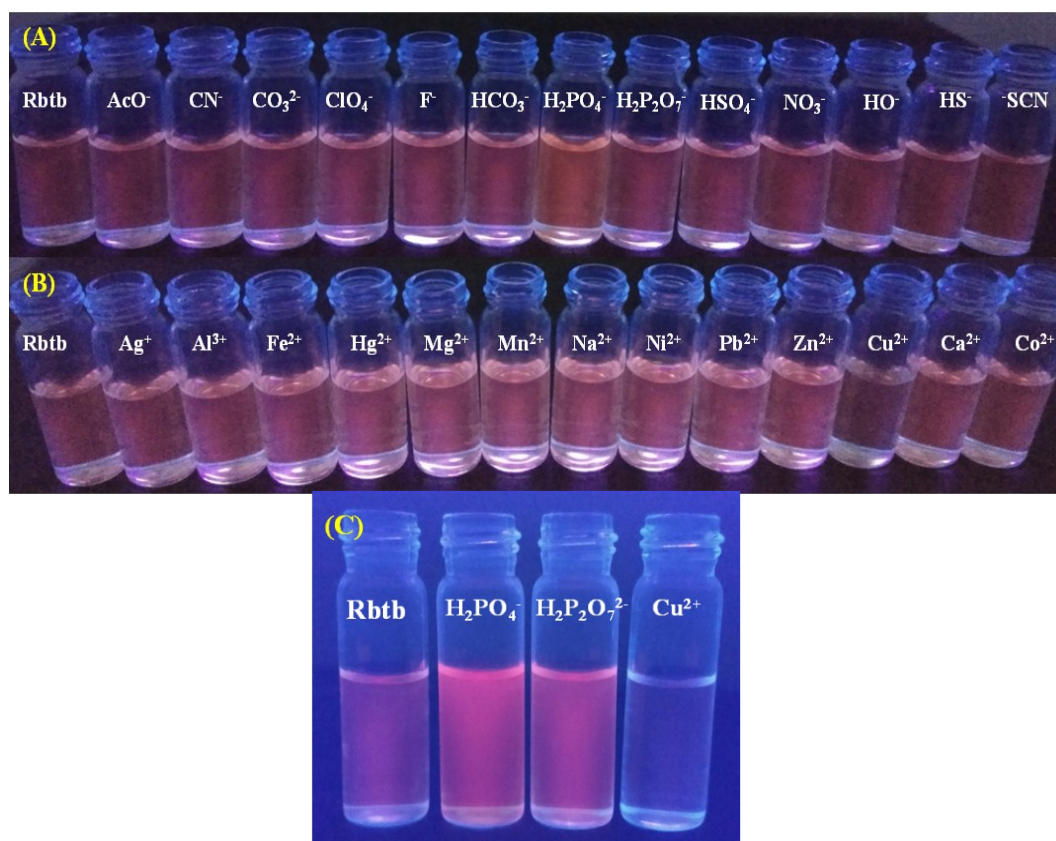


Fig. S17. (A) Under UV light illumination, Rbtb with mentioned other anions (B) Under UV light illumination, Rbtb with mentioned other metal ion (C) Under UV light illumination, closer look image of Rbtb, Rbtb+ $H_2PO_4^-$, Rbtb+ $H_2P_2O_7^{2-}$ and Rbtb+ Cu^{2+}

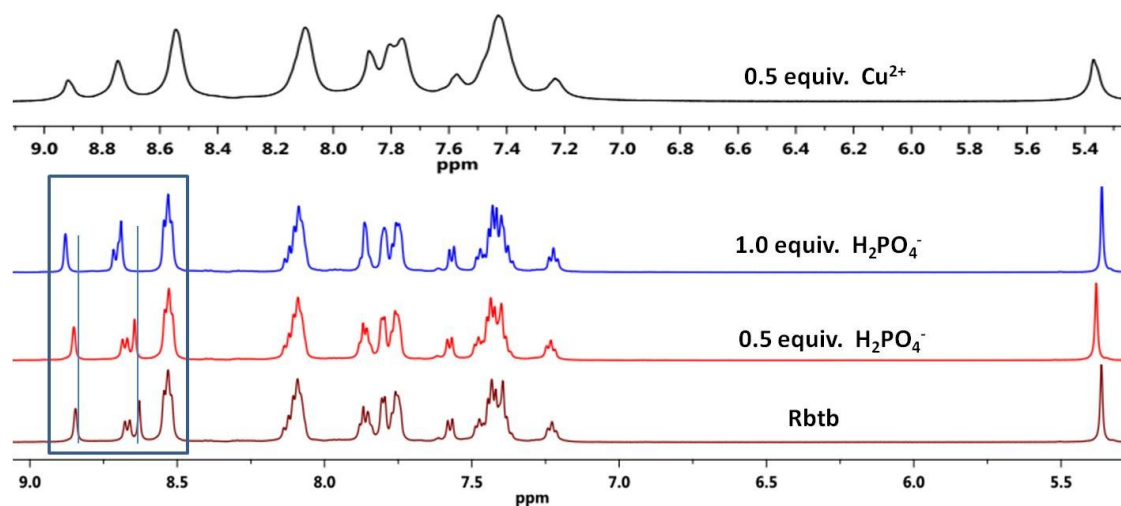


Fig. S18. NMR titration of Rbtb (4.5 mM) with H_2PO_4^- in $\text{CD}_3\text{CN}/\text{CD}_3\text{OD}$ (9/1, v/v)

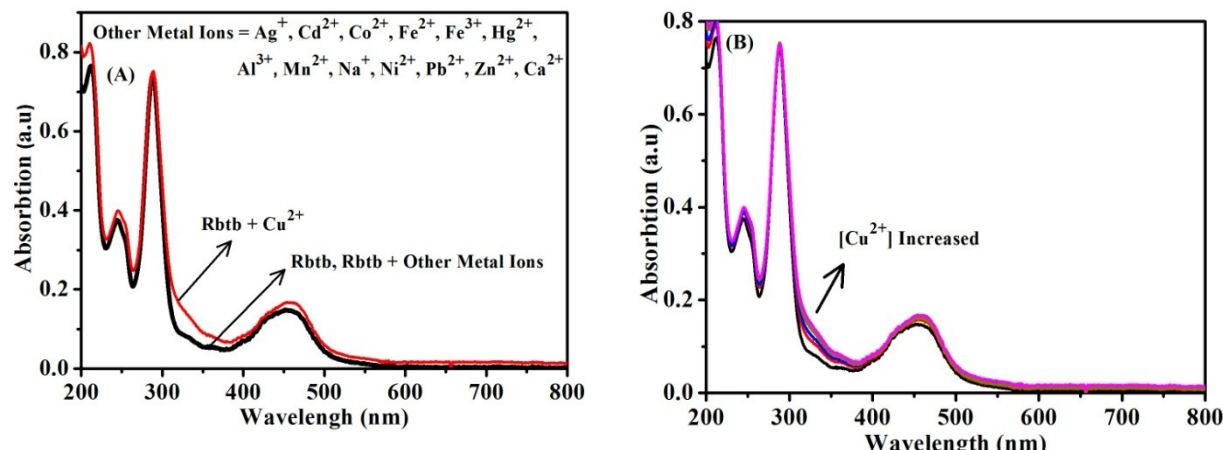


Fig. S19. (A) UV-Vis spectra of Rbtb (10 μM) with variety of metal ions (10 equiv.) and (B) UV-Vis spectra of Rbtb (10 μM) with gradual addition of two equiv. of Cu^{2+} ions in $\text{CH}_3\text{CN}/10$ mM HEPES buffer (pH = 7.4) (9/1, v/v)

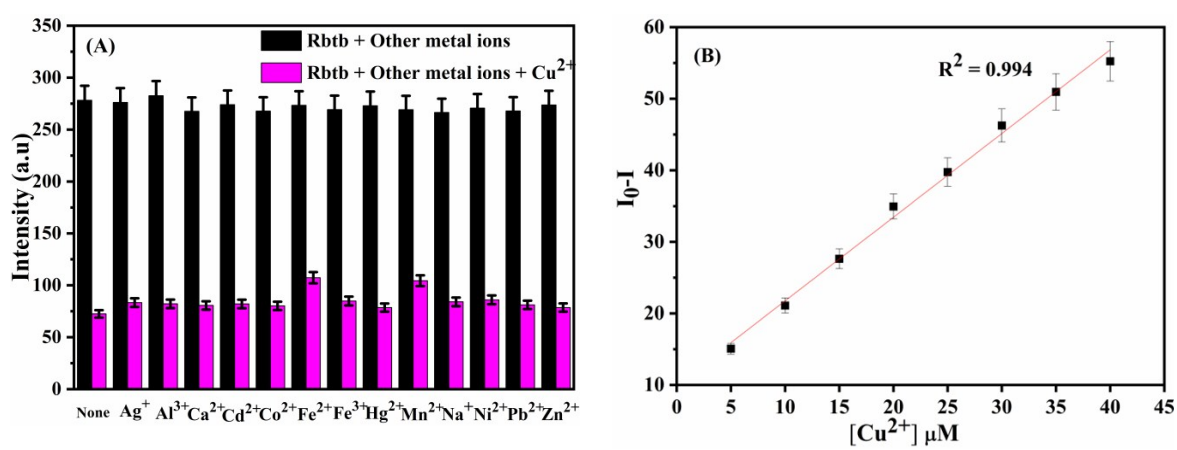


Fig. S20. (A) Interference study of Rbtb (10 μM) + Cu^{2+} (2 equiv.) with mentioned other metal ions (10 equiv.) (B) Linear plot of Rbtb- Cu^{2+}

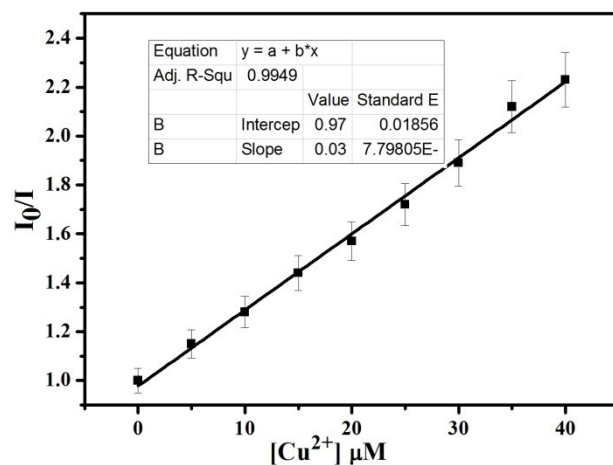


Fig. S21. Stern-Volmer plot for the detection of Cu^{2+} ion by relative fluorescence Rbtb in $\text{CH}_3\text{CN}/10\text{mM}$ HEPES buffer (pH = 7.4).

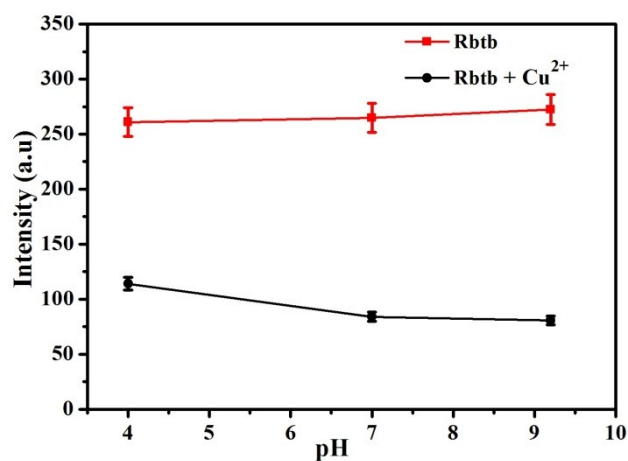


Fig. S22. pH variation was monitored with Rbtb, Rbtb- Cu^{2+}

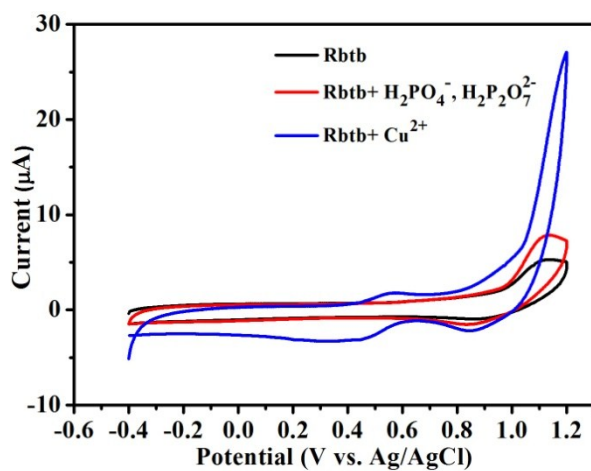


Fig. S23. The cyclic voltammogram of Rbtb, with phosphate and with copper (II) ions

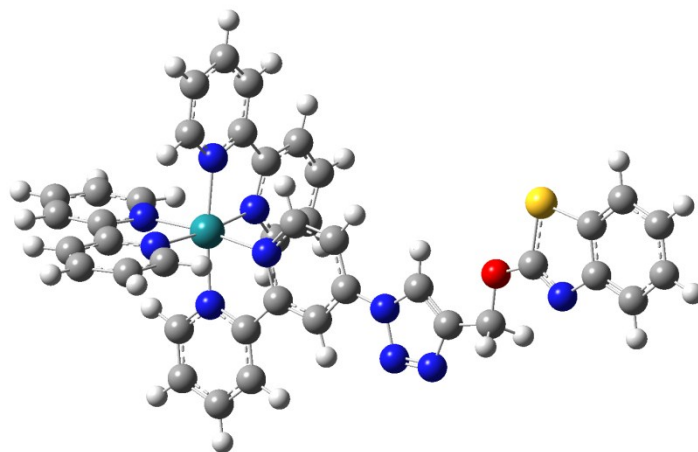


Fig. S24. Optimized geometry of Rbtb

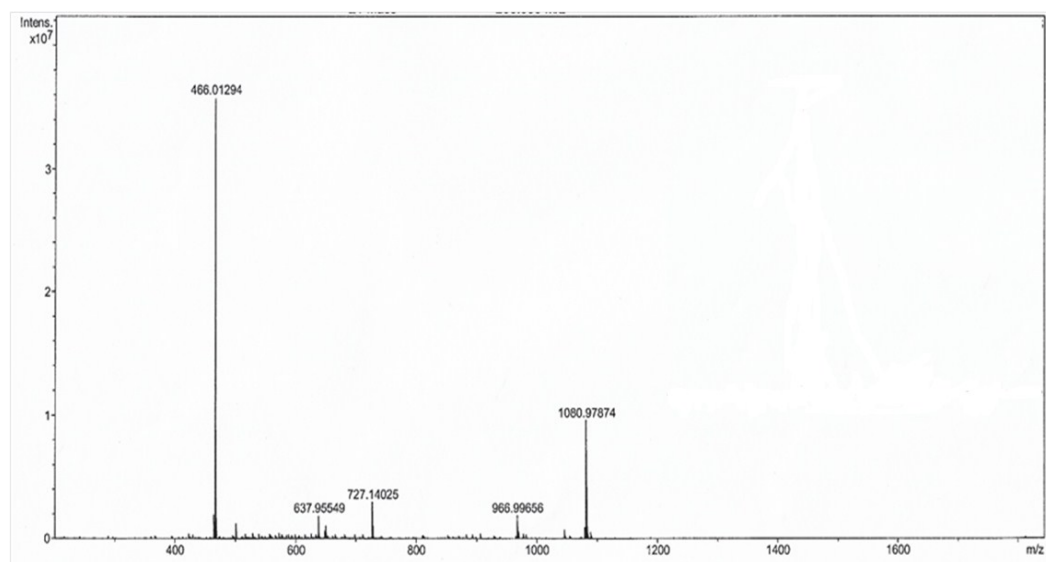


Fig. S25. HRMS of $[\text{Rbtb-Cu}^{2+}]$ adduct $\{[\text{C}_{40}\text{H}_{30}\text{Cl}_2\text{CuN}_{10}\text{ORuSPF}_6]^{2+}\}$: Calcd: $M = 1079.98$; Found: $[\text{M}]^+ = 1080.97$

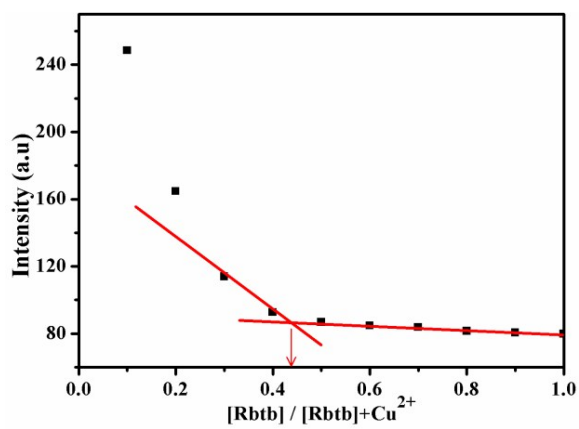


Fig. S26. Job's plot for Rbtb-Cu^{2+}

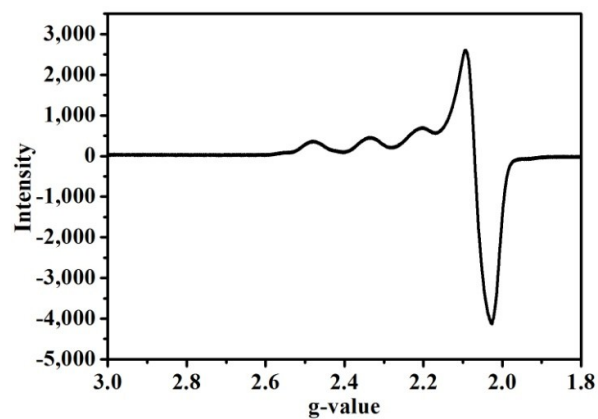


Fig. S27. EPR spectrum of Rbtb-Cu²⁺ at LNT

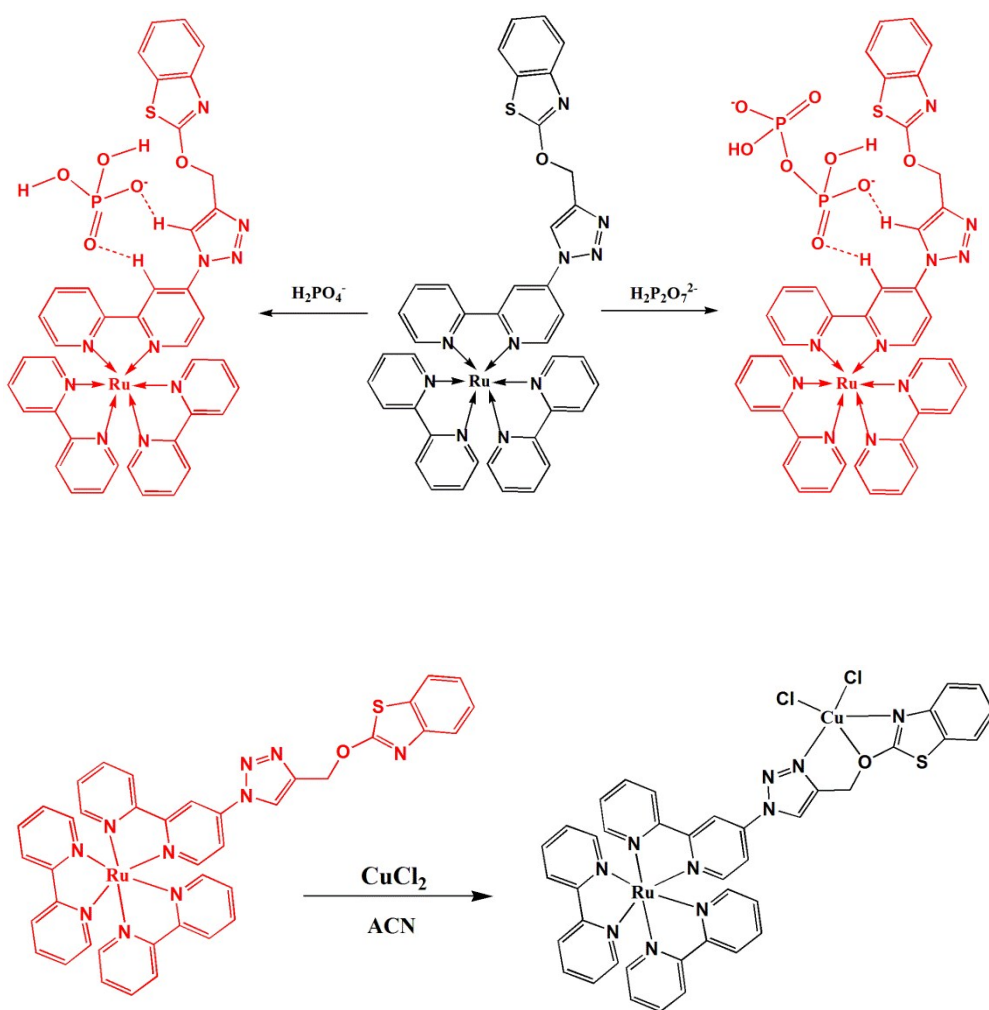
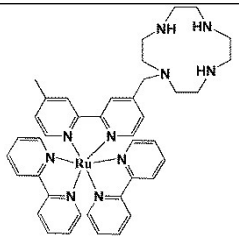
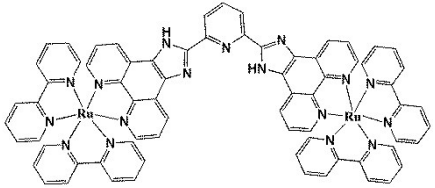
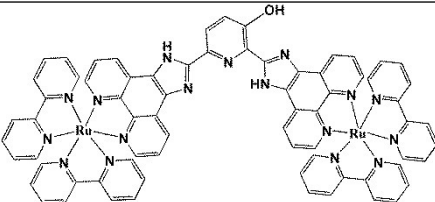
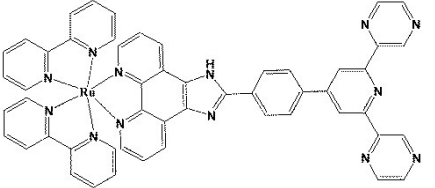


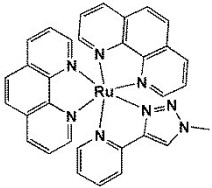
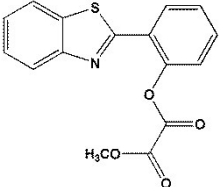
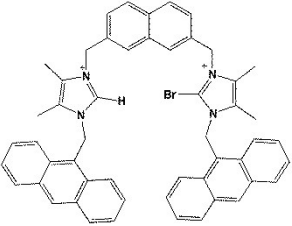
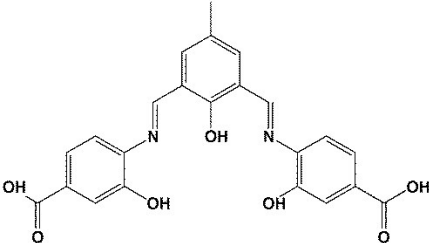
Fig. S28. Proposed mechanism of Rbtb- H_2PO_4^- , Rbtb- $\text{H}_2\text{P}_2\text{O}_7^{2-}$ (above) and Rbtb-Cu²⁺ (below)



Fig. S29. DAPI staining of (A) MCF-7 cell lines (C) Rbtb treated MCF-7 cell line images under fluorescent spectra and (B) Normal image of MCF-7 cell lines.

Table S1. Comparative table for detection limit with existed sensing probes

Probe Structure	Detected Ion (Copper, phosphate) and detection Limit	Reference
	Cu ²⁺ and 5.4 μM	<i>-Dalton Trans.</i> , 2013, 42 , 13509-13515.
	Cu ²⁺ and 0.08 μM	<i>-Chem. Eur. J.</i> , 2013, 19 , 15494-15503.
	Cu ²⁺ and 0.87 μM	<i>-Sensors and Actuators B</i> , 2017, 253 , 203-212.
	Cu ²⁺ and 2.73 μM	<i>-Sensors and Actuators B</i> , 2015, 211 , 449-455.

	$\text{H}_2\text{PO}_4^{2-}$ and 0.25 μM ; $\text{HP}_2\text{O}_7^{3-}$ and 0.45 μM	- <i>Inorg. Chem.</i> 2014, 53 , 8061-8070.
	$\text{H}_2\text{PO}_4^{2-}$ and 0.806 μM	- <i>Chin. J. Chem.</i> , 2018, 36 , 1179-1181.
	$\text{H}_2\text{PO}_4^{2-}$ and 3.9 μM	- <i>Molecules</i> , 2017, 22 , 2273 (1-11).
	$\text{H}_2\text{PO}_4^{2-}$ and 3.5 μM	- <i>Org. Biomol. Chem.</i> , 2013, 11 , 1537–1544.
In this Work	Cu^{2+} and 0.70 μM ; $\text{H}_2\text{PO}_4^{2-}$ and 0.22 μM ; $\text{H}_2\text{P}_2\text{O}_7^{2-}$ and 0.31 μM	---

References

- S1. K. M. Hosamani and R. V. Shingalapur, *Arch. Pharm. Chem. Life Sci.* 2011, **11**, 311-319.
 S2. M. Ramachandran, S. Anandan and M. Ashokkumar, *New J. Chem.*, 2019, **43**, 9832-9842.
 S3. B. S. Uppal, A. Zahid, P. I. P. Elliott, *Eur. J. Inorg. Chem.*, 2013, 2571-2579.